Sergey S. Petrov* and Nikolay G. Iakovlev

The suite of Taylor–Galerkin class schemes for ice transport on sphere implemented by the INMOST package

https://doi.org/10.1515/rnam-2021-00..
Received May 27, 2021; accepted ..., 2021

Abstract: Realizations of the numerical solution of the scalar transport equation on the sphere, written in divergent form, are presented. Various temporal discretizations are considered: the one-step Taylor–Galerkin method (TG2), the two-step Taylor–Galerkin method of the second (TTG2), third (TTG3), and fourth (TTG4) orders. The standard Finite-Element Galerkin method with linear basis functions on a triangle is applied as spatial discretization. The flux correction technique (FCT) is implemented. Test runs are carried out with different initial profiles: a function from C_∞ (Gaussian profile) and a discontinuous function (slotted cylinder). The profiles are advected by reversible, nondivergent velocity fields, therefore the initial distribution coincides with the final one. The case of a divergent velocity field is also considered to test the conservation and positivity properties of the schemes. It is demonstrated that TG2, TTG3, and TTG4 schemes with FCT applied give the best result for small Courant numbers, and TTG2, TTG4 are preferable in case of large Courant number. However, TTG2+FCT scheme has the worst stability. The use of FCT increases the integral errors, but ensures that the solution is positive with high accuracy. The implemented schemes are included in the dynamic core of a new sea ice model developed using the INMOST package. The acceleration of the parallel program and solution convergence with spatial resolution are demonstrated.

Keywords: Finite elements, transport equation, flux correction, Taylor–Galerkin method, INMOST, Ani3D.

MSC 2010: 76M10, 86A05

One of the fundamental problems of computational physics is the construction of an efficient and accurate scheme for the numerical solution of the transport equation. The problem of transporting the characteristics of sea ice, snow and melt ponds on the surface of snow and ice in the finite element model of the evolution of sea ice in the Arctic Ocean being developed at the INM RAS is no exception [13].

Usually, much attention is paid to the description of the ice edge. In addition, high accuracy is important when describing the transport of various categories of ice by thickness (mass and concentration of ice in each category), since characteristics of sea ice, such as strength, depend on the distribution function of ice in gradations of thickness, and thickness is a nonlinear function of mass and concentration. Moreover, the strength of ice affects the characteristics of ice drift and the formation of areas of open water and ice ridges. Statistics reproduction of the share of open water is important for modelling mass and energy exchange between the ocean and the atmosphere, and statistics reproduction of ice ridges is important for navigation problems.

In addition, the features of the ice drift field are such that the velocity changes on relatively small spatial scales, in fact, on the crack width, that is, on scales of 10–1000 m [10]. Satellite data show the presence of extended features (linear kinematic features, LKF), along which high values of vorticity, shear and divergence of the drift velocity are noted [7]. The reproduction of LKF statistics is one of the modern problems of modelling the ice cover of the Arctic [11] and also imposes high demands on the quality of the transport scheme.

One class of transport schemes used in the framework of the finite element method, Taylor–Galerkin schemes, including those with a flux correction method is considered in the present paper. This is the scheme

***Corresponding author: Sergey S. Petrov,** Marchuk Institute of Numerical Mathematics, Russian Academy of Sciences, Moscow 119333, Russia. E-mail: sergey.petrov@phystech.edu
Nikolay G. Iakovlev, Marchuk Institute of Numerical Mathematics, Russian Academy of Sciences, Moscow 119333, Russia

used in the well-proven FESIM 2.0 [4] model. Meanwhile, FESIM 2.0 does not allow the user to choose more accurate schemes, such as, for example, two-step Taylor–Galerkin schemes of the third and fourth order in time. From the point of view of stability, the scheme used in FESIM 2.0 has a Courant number constraint of 0.6 (the estimate was obtained for uniform triangulation and bilinear basis functions [14]), when using strongly non-uniform grids with a locally high spatial resolution, this creates big problems. In the case of uneven triangulation, this estimate should be checked. It seems that an increase in the stability limit of the transport scheme can be important when using the full model of sea ice drift in real forecasting problems, when the computation time becomes fundamental.

The task of the work was to implement and test a set of parallel solvers for computing 2D transport on a sphere (including in the case of an aquaplanet). A revision is made of various methods of the Taylor–Galerkin type for integrating the transport equation written in a divergent form. The Ani3D [2, 8] and INMOST [3, 6, 15] packages, developed at the INM RAS, were used to construct the grids and implement the solvers in software. The code for these libraries is open source and freely distributed. To test various schemes, we used a set of scalar transport tests on the sphere [12]. The test, with a divergent velocity field, which is typical for sea ice, is of the particular interest.

Typically the computational efficiency of the transport scheme is of great importance, since for sea ice approximated by 5 categories of thickness, with 5 levels of the grid inside the ice, the number of transported two-dimensional fields is at least 50 (ice mass, concentration, ice enthalpy profile along thickness, snow mass, surface temperature, concentration of melt ponds — all in each category by ice thickness). Increasing the resolution in thickness and in the number of categories increases the number of fields to be transported. Thus, the problem of transporting the characteristics of ice becomes essential from the point of view of computational resources. The situation is even more complicated when describing the biochemistry of sea ice - the number of transported two-dimensional fields can be at least 200.

The article is organized as follows. In Section 1 a formulation of various Taylor–Galerkin schemes and a numerical implementation by the finite element method are given, then a description of the flux correction procedure is presented. In Section 2 the numerical experiments setups are formulated — the initial distributions of the scalar field on the sphere and the ice drift velocity field. Section 3 describes the features of parallel implementation. In Section 4 the computation results are presented. Section 5 summarizes the conclusions and recommendations on the use of various schemes.

1 Time discretization

Let us consider the scalar transport equation on sphere. Hereinafter, the transported scalar m will be called the mass

$$\frac{\partial m}{\partial t} + \nabla \cdot (m\mathbf{u}) = 0. \tag{1.1}$$

Here $\mathbf{u}$ is the known velocity field that depends on time and assumed to be specified on the whole sphere and smooth enough.

In this section, we will consider various explicit time discretizations of equation (1.1) based on the Taylor expansion. The choice of explicit time discretizations in the finite element ice models is due to the low complexity of the mass matrix inversion and the possibility of using the classical version of the flux correction method [9] to obtain a positive globally conservative solution, which will be discussed below.

1.1 One-step Taylor–Galerkin method of the 2nd order (TG2)

By expanding the mass function in a Taylor series and using equality (1.1) under the assumption of a constant velocity field $\mathbf{u}$ within the time integration step [16], the second order time approximation Taylor–Galerkin

(TG2) method is obtained:

$$m^{n+1} = m^n - \Delta t \nabla \cdot (m^n \mathbf{u}) + \frac{\Delta t^2}{2} \nabla \cdot (\mathbf{u} \nabla \cdot (m^n \mathbf{u})). \tag{1.2}$$

The last term in (1.2) can be interpreted as diffusion.

1.2 Two-step Taylor–Galerkin method of the 2nd order (TTG2)

We also consider a two-step variation of the standard Taylor–Galerkin method (1.2), which is written as [16]:

$$\begin{aligned} m^{n+1/2} &= m^n - \frac{\Delta t}{2} \nabla \cdot (m^n \mathbf{u}) \\ m^{n+1} &= m^n - \Delta t \nabla \cdot (m^{n+1/2} \mathbf{u}). \end{aligned} \tag{1.3}$$

Both equalities have the same structure up to numerical factors. Therefore, the computational costs for assembling the right-hand sides in the two-step variation (1.3) are less than in the one-step analogue (1.2), since there is no need to discretize the diffusion term with second derivatives. However, this method requires a two-fold solution of the arising systems of linear equations with a mass matrix. Despite the fact that all the arising systems of linear equations are solved with high precision (by the bi-conjugate gradients method with an ILU2 preconditioner with an accuracy of 10^{-9} in the relative residual norm), the computations showed that the assembly time for the right-hand sides of discrete equations significantly exceeds the time for solving the linear systems.

1.3 Two-step Taylor–Galerkin method of the 3rd (TTG3) and 4th (TTG4) order

Let us consider a two-step method of the form

$$\begin{aligned} m^{n+1/2} &= m^n - \frac{1}{3} \Delta t \nabla \cdot (m^n \mathbf{u}) + \alpha \Delta t^2 \nabla \cdot \left[\mathbf{u} \nabla \cdot (m^n \mathbf{u}) \right] \\ m^{n+1} &= m^n - \Delta t \nabla \cdot (m^n \mathbf{u}) + \frac{\Delta t^2}{2} \nabla \cdot \left[\mathbf{u} \nabla \cdot \left(m^{n+1/2} \mathbf{u} \right) \right]. \end{aligned} \tag{1.4}$$

Substituting the first equality (1.4) into the second one can make sure that this two-step method is an approximation of equation (1.1) with the third order in time for any value of the parameter α. In [14], it is shown that the choice of $\alpha = 1/9$ makes the phase velocity of the two-step scheme identical to the one-step and minimizes the amplitude error.

Consider now a two-step method of the form

$$\begin{aligned} m^{n+1/2} &= m^n + \alpha \Delta t \nabla \cdot (m^n \mathbf{u}) + \beta \Delta t^2 \nabla \cdot \left[\mathbf{u} \nabla \cdot (m^n \mathbf{u}) \right] \\ m^{n+1} &= m^n + \Delta t \nabla \cdot (m^{n+1/2} \mathbf{u}) + \gamma \Delta t^2 \nabla \cdot \left[\mathbf{u} \nabla \cdot \left(m^{n+1/2} \mathbf{u} \right) \right]. \end{aligned} \tag{1.5}$$

It was shown in [14] that the choice

$$\alpha = 0.1409714, \quad \beta = 0.1160538, \quad \gamma = 0.3590284$$

gives an approximation of equation (1.1) of the fourth order of accuracy in time.

The computational complexity of one iteration of the two-step method of the third (1.4) and fourth (1.5) orders is greater than the one-step method (1.2) due to the need to solve a linear systems with a mass matrix twice.

1.4 Flux correction method (FCT)

All integration schemes at least of the second order of approximation in time are subject to numerical oscillations. In the core of sea ice dynamics, the appearance of negative mass values is unacceptable. In order to overcome this drawback, explicit schemes are complemented by the flux correction method [9].

All the previously described high-order time schemes (1.2)–(1.5), after spacial discretization, take the form

$$\mathrm{M}\Delta\mathbf{m}^H = \mathbf{r} \tag{1.6}$$

with mass matrix M, right-hand size vector $\mathbf{r}$ and the vector of the difference of the nodal mass values $\Delta\mathbf{m}^H = \mathbf{m}^H - \mathbf{m}^n$, where $\mathbf{m}^H$ and $\mathbf{m}^n$ are the nodal mass values obtained according to the high-order scheme and from the previous step, respectively.

In addition to the corresponding high-order scheme, the Löhner scheme is constructed — a first-order scheme with a lumped mass matrix ($\mathrm{M_L}$) and a right-hand side with artificial diffusion

$$\mathrm{M_L}\Delta\mathbf{m}^L = \mathbf{r} + c_d(\mathrm{M} - \mathrm{M_L})\mathbf{m}^n. \tag{1.7}$$

The local difference between high and low order solutions determines the numerical fluxes that is created on the element. Then the low-order solution at each node is adjusted to account for the fluxes from adjacent elements. The described method ensures the fulfillment of the condition $m_i^L \leqslant m_i^{n+1} \leqslant m_i^H$ at each node of the computational grid, where m_i^L and m_i^H are the solutions at the ith node obtained from low and high order schemes, and m_i^{n+1} is the solution obtained using flux correction. This guarantees the positiveness of the mass, in the case of the positiveness of the solution obtained by the low-order scheme (in our case, the choice of $c_d = 0.5$ provided the positiveness). However, in practice, small amplitude oscillations are possible. Also, the flux correction method has the property of global conservativity in the presence of this property in the selected high-order scheme.

2 Initial mass distributions and velocity fields

In the present work, we implement a set of numerical experiments described in [12]. It includes two types of initial mass distributions and three types of reversible velocity fields. The first type of initial field under consideration is Gaussian Hills (GH) — two infinitely smooth Gaussian surfaces located symmetrically about the prime meridian. The second profile is Slotted Cylinders (SC) — two discontinuous mass profiles, also symmetrically located. The described scalar fields of the initial mass distribution are shown in Fig. 1. Initial profiles are set in pairs to check the symmetry of the transport scheme in two hemispheres.

We introduce two types of reversible divergence-free and one divergent velocity field according to [12]. In the case of using reversible divergence-free fields, an exact solution is available that coincides with the initial mass distribution, which allows a quantitative comparison of various numerical integration schemes. The divergent field is used to check whether the solution is globally conservative and positive. The first velocity field implements a divergence-free pair of vortices in the western and eastern hemispheres (ND1). The second velocity field differs from the first by the addition of the zonal velocity component, which transfers the mass along the entire parallel during the integration time (ND2). The third velocity field is the divergent velocity field with mass pumping towards the equator (D). All the described velocity fields at the initial moment of time are shown in Fig. 2.

In the case of comparing the result with the exact solution, the following error values are used. If m is the mass distribution at the final time, and m_i is the initial mass distribution, then the errors are defined as follows [12]:

$$l_1 = \frac{I[|m - m_i|]}{I[|m_i|]}, \qquad l_2 = \left[\frac{I[(m - m_i)^2]}{I[m_i^2]}\right]^{1/2}, \qquad l_\infty = \frac{\max|m - m_i|}{\max|m_i|}$$

$$\varphi_{\max} = \frac{\max(m) - \max(m_i)}{\Delta m_i}, \qquad \varphi_{\min} = \frac{\min(m) - \min(m_i)}{\Delta m_i}$$

where $I[\cdot]$ is the integral over sphere, $\Delta m_i = \max(m_i) - \min(m_i)$. The error values are given in the tables in the github repository [5].

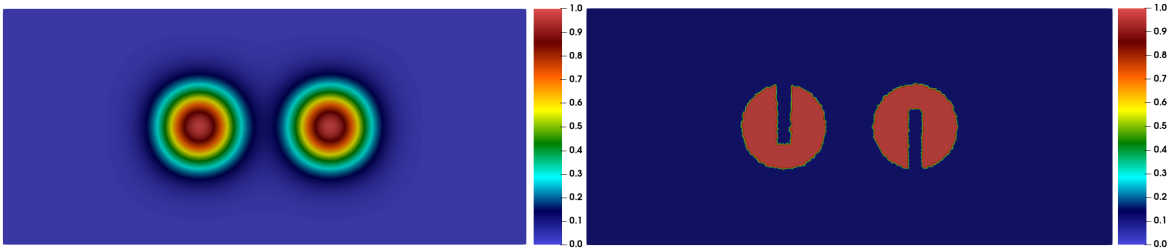

Fig. 1: Initial distribution of mass. Gaussian hills (GH) (left), slotted cylinders (SC) (right).

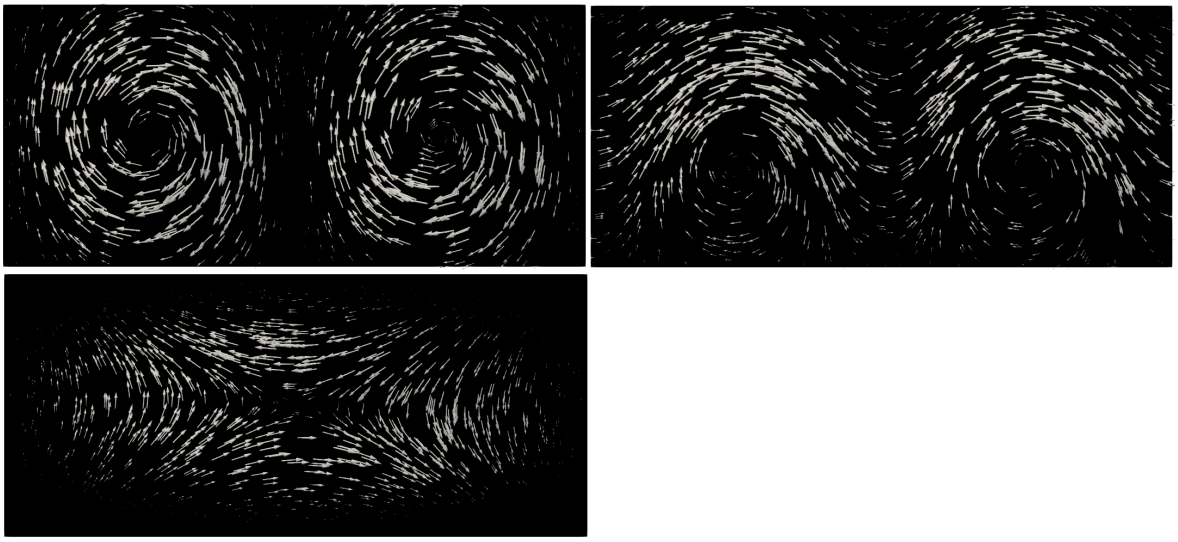

Fig. 2: Test velocity fields. A pair of vortices (ND1) (top left), two-vortex flow with displacement (ND2) (top right), divergent field (D) (bottom).

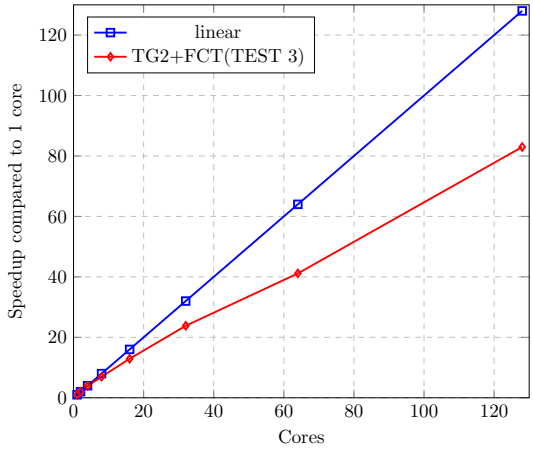

Fig. 3: Acceleration of the parallel program by the example of the TG2+FCT method in Test 3.

3 Spatial discretization and features of parallel implementation

The computational grid is a quasi-regular triangulation of a sphere with the Earth's mean radius. The typical triangle size for most tests is 200 kilometers. Triangulation is made using the Ani3D [2] package. As a spatial discretization, the standard Galerkin method is used, which approximates the unknown function and velocity components by a linear function on a triangle. Test functions are also linear on the triangle. It is known

that this spatial approximation is of the second order on a regular triangular grid. Differential operators are approximated on triangles in a local Cartesian basis. In [1] it is shown that using flat triangles instead of curvilinear ones introduces an additional error in the spatial approximation of the order of (h^2/R^2), where h is the size of the triangle, R is the Earth's radius. Thus, it can be stated with high accuracy that the spatial approximation has the second order.

The parallel code is written in C++ using the library for distributed computing on unstructured grids INMOST [3], which is being developed and maintained at the INM RAS. INMOST software package includes MPI and OpenMP functionality. All tests were executed on 32 processors, however, one can see that there is a scalability property (Fig. 3). The efficiency of a parallel program on 128 processes is about 65%.

4 Numerical experiments

In numerical experiments, schemes with flux correction are mainly investigated. In practice, schemes without flux correction have a stability region that is in good agreement with the estimate given in [14]. For example, in the tables in [5], one can see that the TTG2 scheme is unstable when the Courant number is 0.6. As will be shown below, in the case of using flux correction, most schemes will be stable at Courant numbers up to 1.1. In general, according to the data obtained, the following tendency can be observed: adding flux correction increases the l_2 error by one order on average, but at the same time reduces the errors of the minimum $\varphi_{\min}$ and maximum $\varphi_{\max}$ by several orders.

4.1 Test 1. GH+ND1

The first test implements the mass distribution GH and the two-vortex divergence-free velocity field ND1. Total integration time $T = 300$ hours. Figure 4 shows the mass distribution at distinctive times. The qualitative difference in the numerical solution of schemes with and without flux correction is not visible.

Figure 5 presents a picture of the convergence of the methods with flux correction when the mesh size is refined. The figure shows only the TG2+FCT and TTG4+FCT methods, since the errors of the remaining methods are somewhat larger, but their curves on a logarithmic scale have the same slope angles. Computations show that the described methods converge on average as $h^{1.8}$, where h is the typical size of the triangle. However, there is a tendency for the order of convergence to decrease with increasing resolution.

4.2 Test 2. SC+ND1

The most realistic in a case of the sea ice is the test that implements the transport of the discontinuous mass distribution SC. The second test uses a divergence-free reversible two-vortex velocity field ND1, similar to the field in the first test. As before, the integration time is $T = 300$ hours. The size of the triangle is 200 kilometers. Figure 6 shows the mass distribution at distinctive time moments. This test shows obvious drawbacks of schemes without flux correction - due to the Gibbs effect at time $t = T/2$ there are visible oscillations, while schemes with flux correction keep the mass value in the range from 0 to 1 with high accuracy (possible small oscillations with an amplitude of the order of 10^{-3}).

Figure 7 presents the integral errors of all methods for the current test. It can be seen that, at low Courant numbers, the TTG2+FCT method is significantly inferior in accuracy to the others. However, at Courant numbers close to 1, it gives a more accurate result. This numerical experiment revealed that the stability region of the TTG2+FCT method is somewhat less than 1, while the other methods are stable at the Courant number equal to 1. The errors of the minimum for all methods are comparable and give the order of 10^{-9} at small Courant numbers and 10^{-3} for large ones.

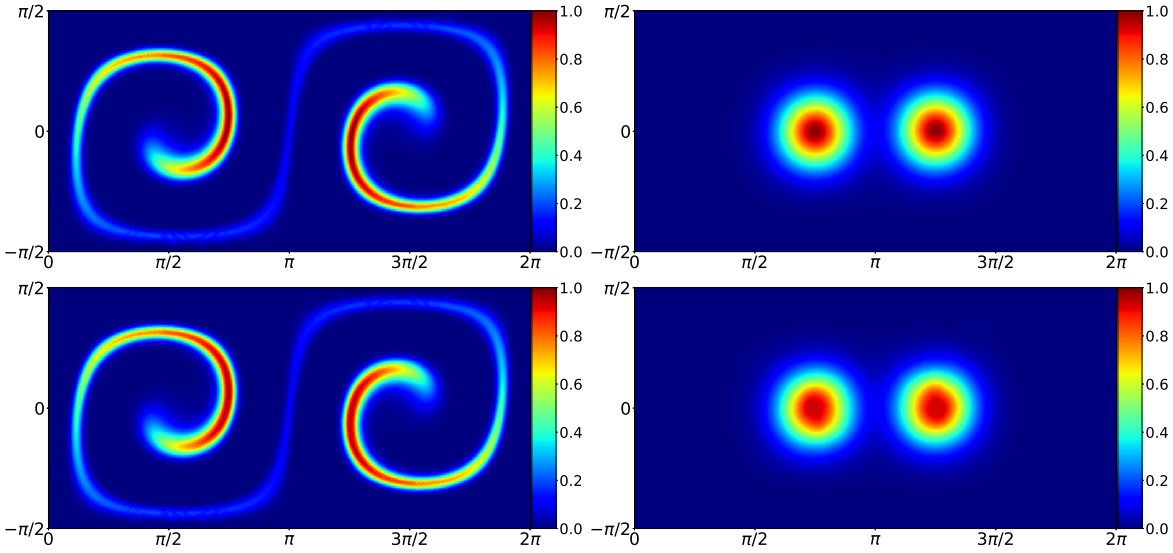

Fig. 4: Test 1: Gaussian hills + ND2, mass distribution at $t = T/2$ (left), $t = T$ (right). TG2 scheme (top), TTG4+FCT scheme (bottom).

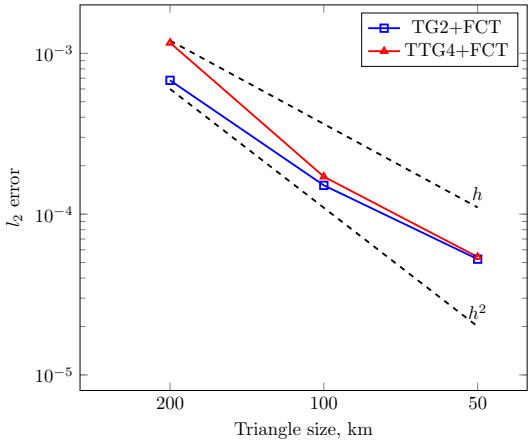

Fig. 5: Picture of convergence in grid spacing.

4.3 Test 3. SC+ND2

Full reversibility of the velocity field can spontaneously suppress the arising oscillations, therefore, a configuration with the same discontinuous initial mass distribution SC is considered, however, a latitudinal component is added to the two-vortex velocity field, which, during the integration time $T = 300$ hours, produces a mass transfer along the circle of latitude (ND2). As in the last test, the size of the triangle is 200 kilometers. The mass distribution is shown in Fig. 8.

Errors for flux-corrected schemes are shown in Fig. 9. As in the previous test, the TTG2+FCT method is distinguished by poor accuracy at small Courant numbers and a smaller stability area. It can be seen that for large Courant numbers, the TTG4+FCT method is most preferred. The minimum errors have a similar order that was described in the second test.

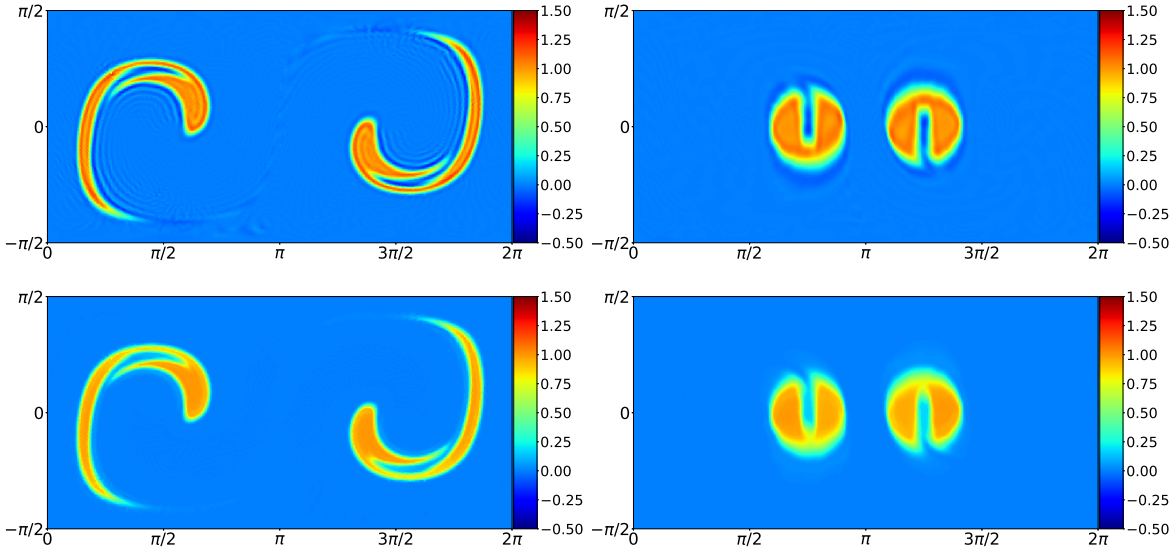

Fig. 6: Test 2: SC+ND1, mass distribution at $t = T/2$ (left), $t = T$ (right). TG2 scheme (top), TTG4+FCT scheme (bottom).

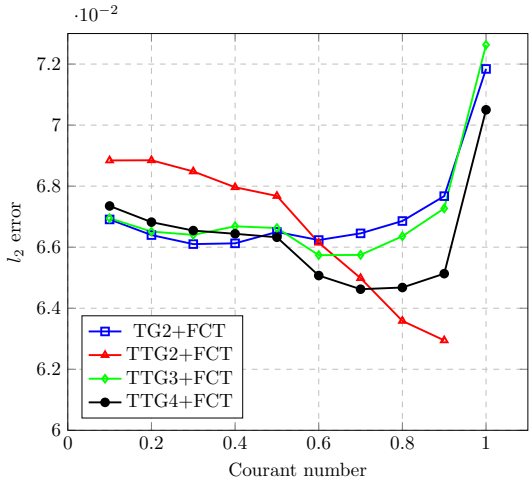

Fig. 7: Test 2: SC+ND1, comparison of integral errors.

4.4 Test 4. SC+D

The last test, which is considered in the present paper, implements the transport of the discontinuous mass distribution SC by the divergent reverse flow D. This test is intended to test the properties of global conservativity and positivity of integration schemes. In the current test $T = 240$ hours, triangle size $h = 200$ kilometers, the Courant number is 0.4. The mass fields at the moment of maximum deformation and the final moment of time are shown in Fig. 10.

Numerical experiments show the global conservativity of all the schemes described above up to machine zero (the ratio of the current mass integral to the initial one is equal to 1). This test clearly demonstrates the positivity property of the flow correction scheme. Figure 11 shows the evolution of the minimum value over time. It can be seen that, with high accuracy, the schemes with flux correction are positive, in contrast to conventional schemes that do not possess this property. At the moment of maximum deformation, the TG2 scheme gives the minimum mass value equal to -2.42, and the TG2+FCT scheme gives a value of the order of 10^{-6}. The absence of huge negative mass is extremely important in physical models. Therefore, in practice, schemes without flux correction are rarely used.

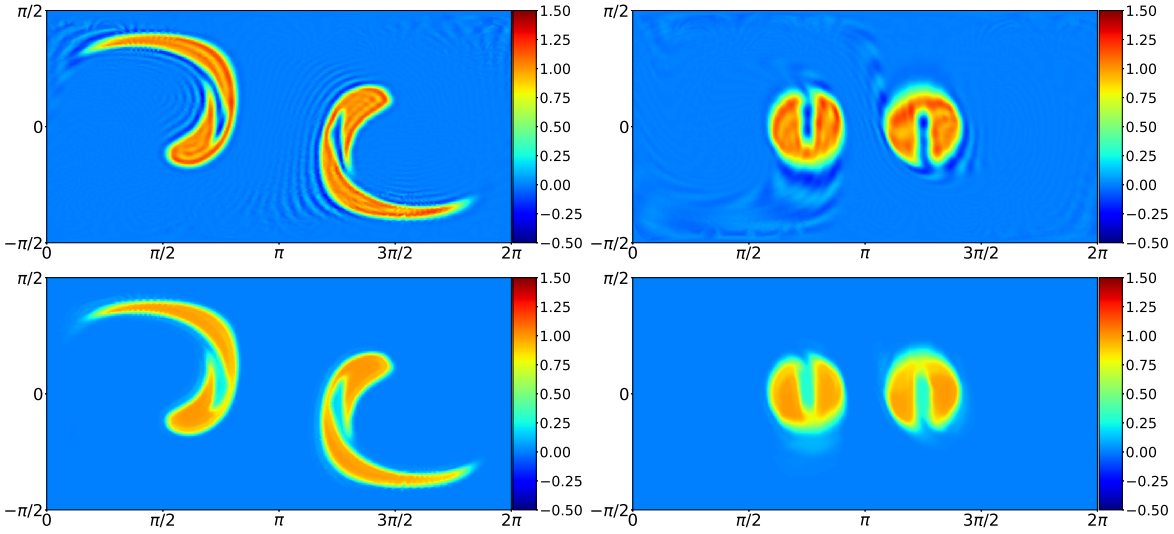

Fig. 8: Test 3: SC+ND2, mass distributions at $t = T/2$ (left), $t = T$ (right). TG2 scheme (top), TTG4+FCT scheme (bottom).

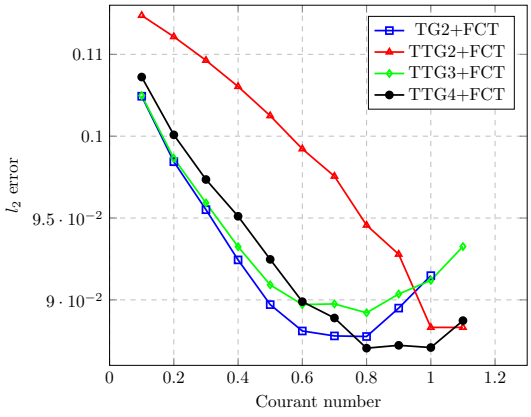

Fig. 9: Test 3: SC+ND2, comparison of integral errors.

5 Summary

For computation the transport of characteristics of sea ice and snow by divergent and non-divergent flows, a set of Taylor–Galerkin-type schemes was implemented using the tools of the INMOST [3] package, using triangulation of sphere made by the Ani3D [2] package. Taylor–Galerkin-type schemes of different order of time accuracy are considered, with and without the flux correction method applied. On each triangle, the integrals are calculated in the local Cartesian basis, which eliminates the problems inherent in spherical coordinates (singularity at the pole, ambiguity at the prime meridian). Each triangle was considered flat, which is justified if the spatial resolution used in practice is not worse than 200 km (the accuracy estimates were made in [1]). Of course, in the case of a real ocean, one can always choose a coordinate system with two or three poles located on the continents, but we have implemented a more general approach. The implemented schemes can be used not only for calculating the dynamics of sea ice, but also, with some generalization to the three-dimensional case, for problems of the dynamics of atmosphere and ocean, and in the configuration of the coupled model of the dynamics of atmosphere and ocean, one can choose conformal grids with different resolutions in each of the media.

The performance and accuracy of the parallel program code was checked on a set of documented tests [12]. The following conclusions can be made:

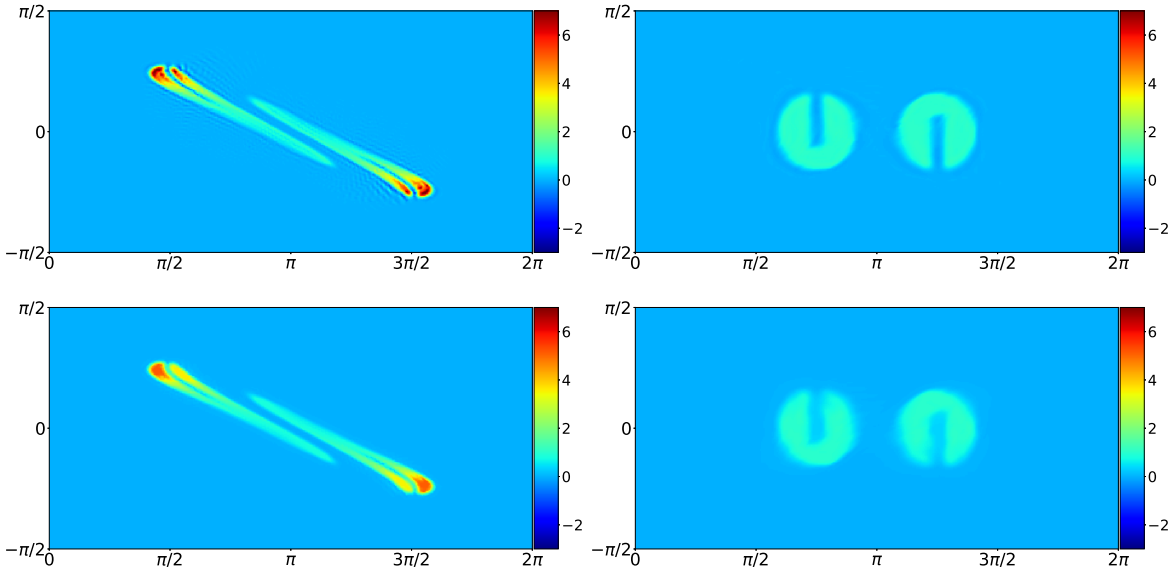

Fig. 10: Test 4: SC+D, mass distributions at $t = T/2$ (left), $t = T$ (right). TG2 scheme (top), TTG4+FCT scheme (bottom).

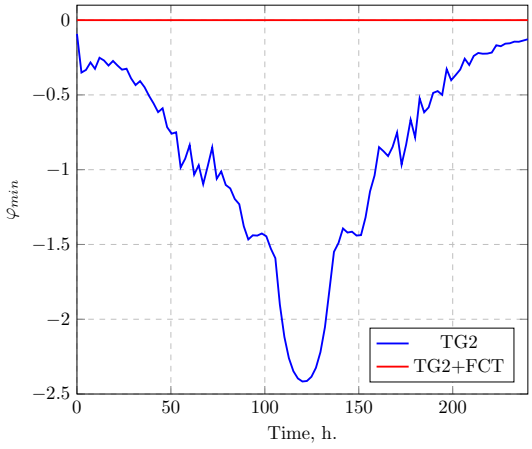

Fig. 11: Test 4: SC+D, evolution of the minimum value of mass over time.

1. The use of the flux correction procedure improves the stability of the scheme in time and ensures the non-negativity of the solution. Qualitatively, the solutions look more realistic, there are no oscillations. In Figs. 7 and 9 it can be seen that most of the flux-corrected schemes are stable at Courant numbers up to 1.1, while conventional schemes tend to be unstable at Courant numbers greater than 0.6, which is reflected in the error tables [5].
2. The high-order schemes TTG3+FCT and TTG4+FCT demonstrate better stability (at Courant numbers up to 1.1–1.2), while the TG2+FCT scheme loses this property at Courant numbers exceeding 1. The scheme TTG2+FCT is more stable than TG2+FCT, however, significantly loses in accuracy to other schemes at low Courant numbers.
3. At low Courant numbers, all schemes give comparable results, with the exception of TTG2+FCT, which is much less accurate. With Courant numbers greater than 0.7, the TTG4+FCT scheme gives the most accurate result. The TTG2+FCT scheme is comparable in accuracy to TTG4+FCT at high Courant numbers, but less stable.
4. According to the performed numerical experiments, it is possible to recommend using the TG2+FCT scheme at low Courant numbers less than 0.5, as it is the least computationally expensive. In the case of large Courant numbers, greater than 0.7, the TTG4+FCT scheme is most preferable, as the most ac-

curate and stable one. The computational complexity of the TTG4+FCT surpasses the TG2+FCT, but the increased accuracy and reliability in terms of stability justifies the cost. This situation is realized in practice in the case of sufficiently small grids or when the grid is refined in the region of the solution singularity or the coastline.

5. The implemented parallel code has approximately linear scalability in terms of the number of processors. Studies with a very large number of processors were not carried out in this work due to the peculiarities of the mesh used in the space of low resolution. Perhaps, in realistic configurations, with a large number of nodes, additional optimization of the parallel code will be required, but this will also depend on the efficiency of the parallel implementation of the block for calculating ice drift velocities. With 128 processors, the code showed an efficiency of about 65%.
6. When using the spatial approximation by the standard Galerkin method with linear basis and test functions on a triangle, in practice the described methods with flux correction give a convergence in the grid step on average of the order of $h^{1.8}$, which was demonstrated in the present work. However, as the resolution increases, the order of convergence decreases, which is typical for transport schemes with a filter.

The use of the flux correction procedure somewhat smooths the solution. This is especially pronounced for the case of a discontinuous initial profile. It should be noted that the degree of dissipativity of the 'low' order scheme is determined by the parameter c_d (see (1.7)), which was fixed at 0.5. At the same time, in the models proposed in [4], this parameter is selected in the range 0.1–0.2. Since the choice of this parameter depends on the specific configuration of the model, the study of the optimality of parameter c_d is left for the future. Also beyond the scope of the paper were questions about the possibility of using lumped mass matrices, at least at the first steps of two-step methods (in this case, the costs of implementing high-order schemes are almost the same as those of the second order), as well as questions of the accuracy of inversion of mass matrices. In this case, the mass matrices were handled with high precision, while in [4, 16] it is proposed to invert the mass matrices by a simple Jacobi iteration method with three iterations. In our opinion, this approach is insufficiently reasoned, and should become the subject of a more detailed study.

It should be noted that this work did not compare the accuracy of the described schemes with other common schemes, which should be the subject of a separate study. The purpose of this work is solely testing and identifying the most applicable Taylor–Galerkin type schemes from the class. Also, the accuracy of the result obtained is significantly affected by the spatial approximation, which can play a primary role, especially at low Courant numbers. Unfortunately, in the finite element paradigm, an increase in the order of spatial approximation entails a significant increase in the number of degrees of freedom. The choice of the described spatial approximation is due to its simplicity and widespread use in the finite element models of sea ice.

Acknowledgment: The authors are grateful to the staff of the INM RAS: Gordey Goyman, Pavel Perezhogin, Vladimir Shashkin, Vasily Kramarenko, and Alexander Danilov for valuable advice and comments, help with the construction of grids and with mastering the INMOST and Ani3D software packages.

Funding: The study was carried out at the INM RAS with the support of the Russian Science Foundation (project 21-71-30023).

References

[1] R. Comblen, S. Legrand, E. Deleersnijder, and V. Legat, A finite element method for solving the shallow water equations on the sphere. *Ocean Modelling* **28** (2009), Issues 1-3.

[2] A. Danilov, Unstructured tetrahedral mesh generation technology. *Comput. Math. Math. Phys.* **50** (2010), 139–156.

[3] A. Danilov, K. Terekhov, I. Konshin, and Y. Vassilevski, Parallel software platform INMOST: a framework for numerical modeling. *Supercomp. Frontiers Innov.* **2** (2015), No. 4, 55–66.

[4] S. Danilov, Q. Wang, R. Timmermann, N. Iakovlev, D. Sidorenko, M. Kimmritz, T. Jung, and J. Schroter, Finite-element sea ice model (FESIM), version 2. *Geoscientific Model Development* **8** (2015), No. 6, 1747–1761.

[5] Error values for Finite Element advection tests on sphere. https://github.com/chuck97/FEtransport_results
[6] INMOST: a toolkit for distributed mathematical modelling. http://www.inmost.org
[7] R. Kwok and D. Sulsky, Arctic Ocean sea ice thickness and kinematics: satellite retrievals and modeling. *Oceanography* **23** (2010), No. 4. 134–143.
[8] K. Lipnikov, Yu. Vassilevski, A. Danilov et al., *Advanced Numerical Instruments 3D*. http://sourceforge.net/projects/ani3d
[9] R. Löhner, K. Morgan, J. Peraire, and M. Vahdati, Finite element flux-corrected transport (FEM-FCT) for the Euler and Navier–Stokes equations. *Int. J. Numer. Meth. Fluids* **7** (1987), 1093–1109.
[10] S. Marcq and J. Weiss, Influence of sea ice lead-width distribution on turbulent heat transfer between the ocean and the atmosphere. *The Cryosphere* **8** (2012), 143–156.
[11] C. Mehlmann, S. Danilov, M. Losch, J. F. Lemieux, N. Hutter, T. Richter, P. Blain, E. C. Hunke, and P. Korn, *Simulating linear kinematic features in viscous-plastic sea ice models on quadrilateral and triangular grids.* arXiv:2103.04431v. 7 Mar 2021.
[12] R. D. Nair and P. H. Lauritzen, A class of deformational flow test cases for linear transport problems on the sphere. *J. Comput. Phys.* **229** (2010), 8868–8887.
[13] S. Petrov and N. Iakovlev, *The optimized Finite Element dynamical core of the Arctic Ocean sea ice model. Commun. Computer Inform. Sci.*, 2021 (in press).
[14] L. Quartapelle, *Numerical solution of the incompressible Navier–Stokes equations, Vol. 113*. Birkhäuser, 1993.
[15] Y. Vassilevski, K. Terekhov, K. Nikitin, and I. Kapyrin, Parallel Finite Volume Computation on General Meshes. Springer, Cham, 2020.
[16] O. C. Zienkiewicz and R. L. Taylor, *The Finite Element Method, Fifth Edition. Vol. 3: Fluid Dynamics*. Oxford, Butterworth–Heinemann, 2000.